Particle Simulation of an Ultrarelativistic Two-Stream Instability

M. E. Dieckmann*

Department of Theoretical Space and Astrophysics, Ruhr-University Bochum, 44780 Bochum, Germany

(Received 25 October 2004; published 20 April 2005)

A two-stream instability in an unmagnetized plasma is examined by a particle-in-cell simulation. Each beam initially consists of cold electrons and protons that stream at a relative Lorentz factor 100. This is representative for plasma close to the external shocks of gamma-ray bursts. An electrostatic wave develops which saturates by trapping electrons. This wave collapses and the resulting electrostatic turbulence gives an electron momentum distribution that resembles a power law with a spectral break. Some electrons reach Lorentz factors over 1000.

DOI: 10.1103/PhysRevLett.94.155001 PACS numbers: 52.35.Fp, 52.65.Rr, 98.70.Sa

Gamma-ray bursts (GRBs) and the relativistic jets of active galactic nuclei (AGNs) are potential sources of highly energetic cosmic ray radiation [1]. The mechanisms that accelerate particles to such energies are probably connected to plasma colliding at highly relativistic speeds. The free energy of the relativistic flow is converted into electrostatic and electromagnetic fields by plasma instabilities which in turn accelerate particles.

In [2–5] streaming instabilities are considered that develop between a plasma at rest and a plasma beam that moves at a mean speed v_b with $\gamma(v_b) = (1 - v_b^2/c^2)^{-0.5} \approx 10^1$–$10^3$. Such relativistic bulk flows probably exist at the external shocks of GRBs where the GRB blast shell encounters the interstellar medium (ISM). Typical flow speeds of relativistic AGN jets are probably found in the lower end of this interval and plasma flow at pulsars may reach much higher $\gamma(v_b) \approx 10^7$ [1].

The large-scale nonlinear evolution of a collision between a GRB blast shell or an astrophysical jet and the ISM can be examined by hydrodynamic simulations [4]. Such simulations can however not resolve the small-scale microinstabilities discussed in [3] for which particle-in-cell (PIC) codes [5,6] are more suitable.

In this work we approximate the interaction between relativistically expanding shells and the ISM plasma by two interpenetrating spatially homogeneous beams. The simulation model is similar to that in [5]. Each beam consists of electrons and protons and we thus introduce 4 plasma species that are distributed uniformly over the one-dimensional simulation box. We examine the developing electrostatic streaming instability, its saturation mechanism and the resulting electron momentum distribution. Since we exclude spatial changes in the initial plasma distribution we exclude potentially important effects arising from the front of the blast shell but this allows us to introduce simple periodic boundary conditions for the simulation. We consider an unmagnetized plasma, which is only realistic if the relativistic shell expands along the magnetic field lines and if the plasma parameters are such that the electrostatic instability grows fastest. If the magnetic field is sufficiently weak so that the electric field accelerates the electrons much faster than the magnetic field, this model may also approximate the initial stage of the developing instability.

The electrons and the protons of the blast shell are species 1 and 2, respectively. The electrons and the protons of the ISM are species 3 and 4, respectively. Our simulation box is at rest in the reference frame of the blast shell. The mean speeds of the blast shell species 1 and 2 are thus $\hat{v}_{b,1} = 0$ and $\hat{v}_{b,2} = 0$. The mean speeds of the ISM species 3 and 4 are $\hat{v}_{b,3} = \hat{v}_{b,4} = v_b$ with $\gamma(v_b) = 100$, which is relevant for GRBs and possibly for the relativistic jets of AGNs. The plasma frequencies are $\omega_{p,i} = (e^2 n_i/m_i\epsilon_0)^{0.5}$ where i is the species index and where e, n_i, and m_i are the elementary charge, the density, and the particle mass for the species. The proton to electron mass ratio is $m_p/m_e = 1836$. The plasma frequencies in the rest frame of the blast shell are $\omega_{p,1} = 10^5 \times 2\pi/s$, $\omega_{p,2} = \omega_{p,1}\sqrt{m_e/m_p}$, $\omega_{p,3} = \omega_{p,1}\sqrt{\gamma(v_b)/2}$, and $\omega_{p,4} = \omega_{p,2}\sqrt{\gamma(v_b)/2}$. The ISM density $6 \times 10^9/m^3$ in the rest frame of the blast shell is comparable to the value $10^9/m^3$ given in [4]. The blast shell density is twice the ISM density if we measure the densities in the respective rest frames of the species. It is thus less than it is believed to be [2,4]. This low ratio accelerates the growth of the instability compared to a simulation time step and it thus reduces the simulation time required to follow the instability to its saturation. The chosen low density ratio may be representative for a thin and fast blast shell fragment that outruns the main blast shell.

The temperature of all species is $T_i = 1.16 \times 10^6$ K. The thermal speed of species i is $v_{\mathrm{th},i} = \sqrt{k_B T_i/m_i}$ in its rest frame. As we show below the $v_{\mathrm{th},i}$ are relatively small and we can find the unstable electrostatic waves by solving the linear cold plasma dispersion relation

$$\sum_{i=1,2} \frac{\omega_{p,i}^2}{\omega^2} + \sum_{i=3,4} \frac{\omega_{p,i}^2}{\gamma^3(v_b)(\omega - \hat{v}_{b,i}k)^2} - 1 = 0 \quad (1)$$

where k and ω are the wave number and the wave frequency. The large proton inertia implies that initially the

proton contribution to the linear dispersion relation can be neglected. Since $\hat{v}_{b,3} = v_b$ the Eq. (1) reduces to

$$\frac{\omega_{p,1}^2}{\omega^2} + \frac{\omega_{p,3}^2}{\gamma^3(v_b)(\omega - v_b k)^2} - 1 = 0 \qquad (2)$$

Initially $\gamma(v_b)$ is constant and we can solve this equation as in [7]. The frequency of the most unstable electrostatic wave in the blast shell frame is obtained as $\omega_u \approx \omega_{p,1}$, its wave number is $k_u \approx \omega_{p,1} v_b^{-1}$ and its growth rate is $\omega_{im} \approx \gamma^{-1}(v_b)(3\sqrt{3}\omega_{p,3}^2\omega_{p,1}/16)^{1/3}$, which is for our plasma parameters $\omega_{im} \approx 2.5 \times 10^{-2}\omega_{p,1}$.

We resolve the x direction by $M = 2 \times 10^4$ cells, each with a length $\Delta x = 2.25\lambda_{D,1}$ where $\lambda_{D,i} = v_{th,i}\omega_{p,i}^{-1}$ is the Debye length of species i. By this Δx we resolve each wave length $\lambda_u = 2\pi/k_u$ by 200 simulation cells and our simulation box length equals $L = 100\lambda_u$. The time step is $\Delta t \approx 0.015/\omega_{p,1}$. We represent the species 1 by 160 particles per cell (ppc), the species 2 by 90 ppc, the species 3 by 1210 ppc, and the species 4 by 360 ppc.

Figure 1 shows the kinetic energy $E_{k,i}(t)$ of each particle species i and the electrostatic field energy $E_E(t) = \epsilon_0 E_x^2(t)/2$ for the simulation duration of $240T_p$ with $T_p = 2\pi\omega_{p,1}^{-1}$.

Figure 1(a) shows that $E_{k,1}$ initially oscillates due to a periodic energy exchange with E_E. The oscillations of E_E are not visible in Fig. 1(a) due to the chosen dynamical range, but we show them below. At $t \approx 70T_p$, $E_{k,1}$ and E_E have identical energies. E_E saturates at $t \approx 75T_p$. At this time $E_{k,2}$ starts to grow. Both $E_{k,1}$ and $E_{k,2}$ continue to grow after E_E has saturated. As the time approaches $240T_p$, $E_{k,2}$ and E_E seem to converge. We obtain $E_{k,2}(240T_p)/E_E(240T_p) \approx 0.7$. The blast shell electrons have increased their energy during the simulation by a factor 2.3×10^5 and $E_{k,1}(240T_p)/E_{k,2}(240T_p) \approx 380$. The energy the $E_{k,1}$, $E_{k,2}$, and E_E components gain is provided by species 3. Most of the energy extracted from species 3, however, flows into species 4 as shown in Figs. 1(b) and 1(c). During the simulation an electromagnetic wave has been growing. The ratio of its energy with the weakest relevant energy $E_{k,2}$ has at no time exceeded 2.5×10^{-3} and we neglect it here.

To confirm that the two-stream instability is responsible for the growth of E_E after $t \approx 50T_p$ and to find the origin of the initial oscillations in E_E and $E_{k,1}$ we calculate the power spectrum

$$E_x^2(k_j, t) = M^{-2}\left|\sum_{l=1}^{M} E_x(x_l, t)\exp(ik_j x_l)\right|^2 \qquad (3)$$

where l is the index of the simulation cell, $x_l = l\Delta x$ and $k_j = 2\pi j/M\Delta x$. We show the wave spectrum in Fig. 2.

In our simulation we could not match exactly the densities of species 3 and 4 mainly due to round-off errors and the random particle momentum initialization. The resulting net current produces the wave with $k = 0$ shown in Fig. 2. Such a net current may not necessarily be unphysical, we may find that also at astrophysical jets over the short spatial range considered here. The power averaged over a time T_p of the mode with $k = 0$, remains constant and low and we do not further discuss it here. This wave causes, by its interaction with the blast shell electrons, the oscillations of $E_{k,1}$ in Fig. 1(a).

We find a wave that grows over a limited wave number band close to k_u with an experimentally measured exponential growth rate Γ_{im} such that $\Gamma_{im}/\omega_{im} \approx 0.95$. The

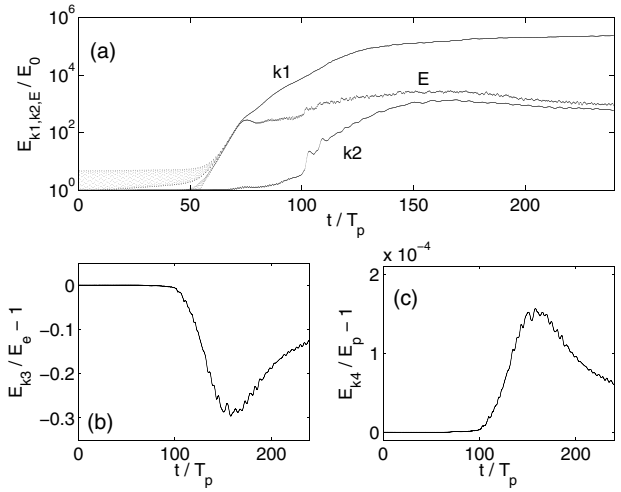

FIG. 1. (a) shows the energies $E_{k,1}$, $E_{k,2}$, and E_E in units of $E_0 = k_b T_1$. Until $t = 50T_p$ we find rapid oscillations of $E_{k,1}$ shown by the broad distribution of values. (b) shows the relative change in $E_{k,3}$ with $E_e = 1.69 \times 10^7 E_0$ and the relative change in $E_{k,4}$ is shown in (c) with $E_p = 3.11 \times 10^{10} E_0$.

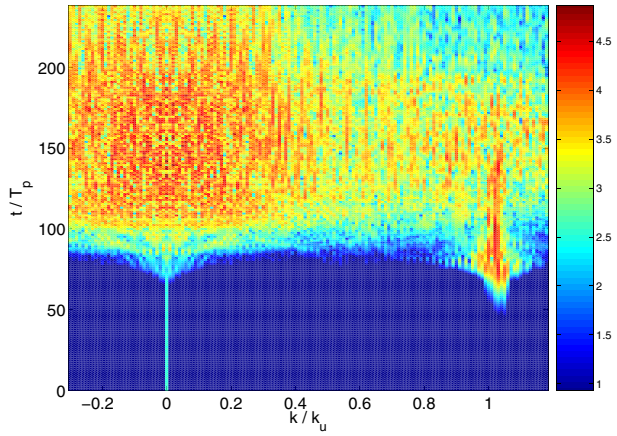

FIG. 2 (color online). The power spectrum $\log_{10}E_x^2(k, t)$ is shown in units of V^2/m^2. Initially only a wave with $k = 0$ is found. Later a wave grows exponentially at $k \approx k_u$. It reaches a peak power of $10^{4.7}$ V^2/m^2 at $t \approx 75T_p$. It maintains a large amplitude until $t \approx 150T_p$ and then it collapses. Simultaneously we observe waves over the entire shown band of k after $t \approx 80T_p$.

solution of Eq. (2) yields such a band [5]. We must also expect changes in the most unstable k due to modulations of the γ factor in Eq. (2) by the wave potential. Both the wave number and the growth rate of the instability are thus in good agreement with the solution of Eq. (2). The wave saturates and is in an equilibrium during $75T_p < t < 150T_p$. Waves grow simultaneously over the entire shown k interval. At the time $t \approx 150T_p$ the wave with $k \approx k_u$ collapses. This coincides with the time in Fig. 1 at which $E_{k,2}$, $E_{k,3}$, and $E_{k,4}$ reach their extrema. The growth of $E_{k,1}$ after $t \approx 150T_p$ must be attributed to electron acceleration by the broadband fluctuations in Fig. 2. To identify the saturation mechanism of the wave at k_u, we show the plasma distribution in a simulation box interval with length λ_u at $t \approx 78T_p$ in Fig. 3.

Species 1 in Fig. 3(a) shows a beam that has been trapped by the wave with $k = k_u$ [8] while species 2 is unaffected. Species 3 and 4 show momentum oscillations with the period λ_u that are shifted by the phase angle π. These asymmetric oscillations account for the changes in $E_{k,3}$ and $E_{k,4}$ in the Figs. 1(b) and 1(c).

The blast shell electrons reach a maximum $\gamma \approx 30$ which shows that the electrons gyrate around a wave potential that is moving with $1 < \gamma < 30$ in the rest frame of the blast shell. Since the rest frames of the ISM and of the blast shell move at $\gamma(v_b) = 100$ relative to each other, the potential moves with a significantly higher γ in the rest frame of the ISM. In the wave's rest frame the blast shell electrons thus have a lower γ than the ISM electrons and they can be trapped more easily. From Fig. 3 we further find that the wave phase speed measured in the reference frame of any species i must be much higher than $v_{\mathrm{th},i}$, justifying the cold plasma approach for Eq. (1).

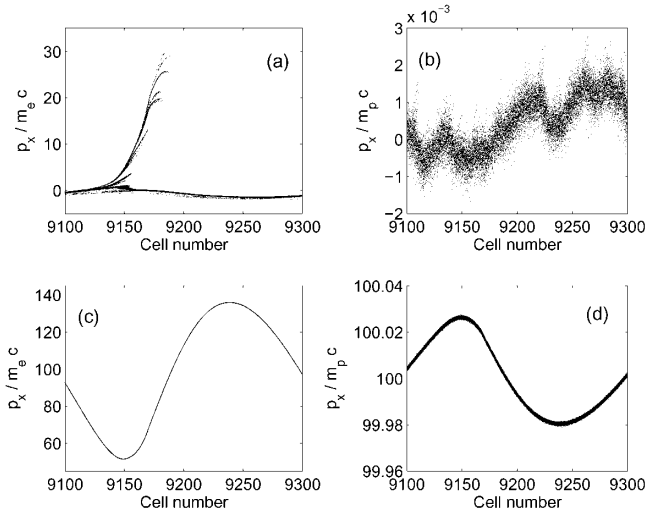

FIG. 3. (a) The distribution of species 1 in a box interval. We find trapped electrons. The distribution of species 2 is shown in (b). No reaction of the blast shell protons to the wave potential is found. The ISM species 3 and 4 are shown in (c) and (d), respectively, both showing momentum oscillations.

The wave with $k = k_u$ is stable between $75T_p < t < 150T_p$ and it forms the relativistic equivalent of a Bernstein-Greene-Kruskal (BGK) mode [9] with species 1. This mode probably collapses due to the sideband instability [10]. We show the accumulated electron phase space distribution of the ISM and the blast shell electrons in a box subinterval at $t = 240T_p$ in Fig. 4. The phase space density $N_e(x, p_x)$ is the electron charge density per phase space interval in units of e.

The electron distribution in Fig. 4(a) shows fluctuations that reach peak values with $\gamma > \gamma(v_b)$. These fluctuations have large variations in their peak γ and in their spatial separation. The distribution at other simulation box intervals is similar. The peak value reached by these spikes in the box is $\gamma \approx 16\gamma(v_b)$. At low γ the distribution $N_e(x, p_x)$ shows in Fig. 4(b) a slowly varying density which is constituted by the blast shell electrons and by a few ISM electrons that have been scattered by the electrostatic potential. The trapped blast shell electrons have been accelerated up to $\gamma \approx 0.3\gamma(v_b)$ and scattered by the collapse of the wave with $k = k_u$ to higher energies and into a smooth distribution. The wave collapse could not scatter the bulk of the ISM electrons and has instead forced it onto a highly oscillatory phase space path which forms an upper bound in p_x for $N_e(x, p_x)$.

The large box length of $100 \times \lambda_u$ should yield a statistically significant number of the spikes shown in Fig. 4 and the 2.7×10^7 computational electrons should accurately resolve the distribution. We count the electrons of species 1 and 3 in each momentum interval, where the width of the interval increases exponentially as a function of p_x to compensate for the decreasing particle number density and statistical accuracy. The charge of each computational

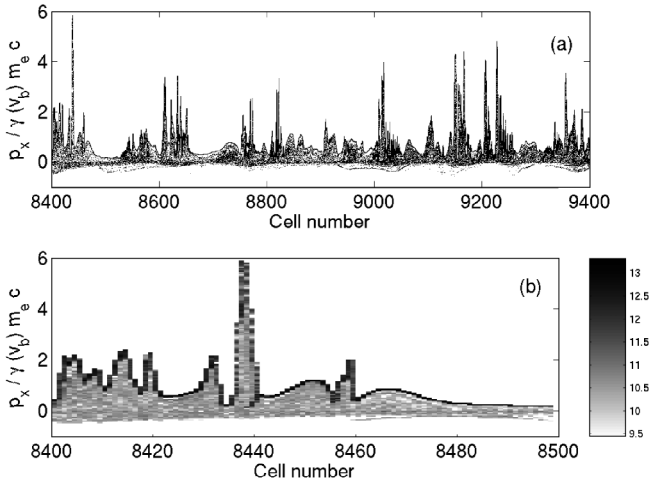

FIG. 4. (a) shows a section of the electron phase space distribution at $t = 240T_p$, each electron being a point. At $1 < \gamma < \gamma(v_b)$ the electron distribution is dense. We find spikes that reach a peak value $\gamma \approx 6\gamma(v_b)$. (b) shows $\log_{10}[N_e(x, p_x)]$. We find a smooth distribution at low γ which is bounded at high γ by a dense beam.

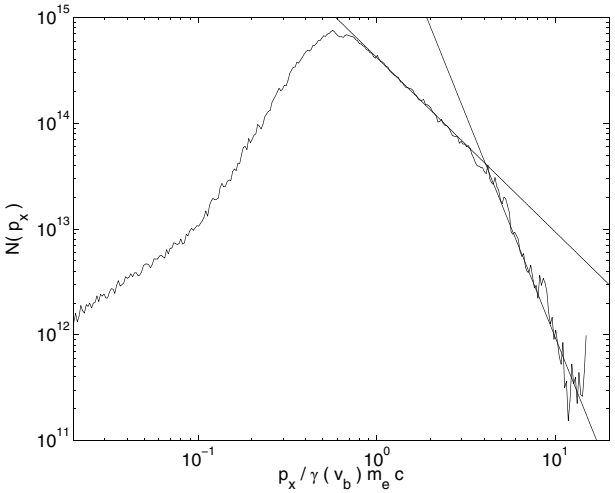

FIG. 5. The accumulated momentum distribution of species 1 and 3 at $t = 240T_p$. The distribution steadily increases up to $\gamma \approx 0.4\gamma(v_b)$ above which the momentum distribution decreases in form of a power law with the exponent -1.3 up to $\gamma \approx 4\gamma(v_b)$. The power law changes into a second one with the exponent -4.2 and we obtain a peak factor $\gamma \approx 16\gamma(v_b)$.

electron is normalized to e. In Fig. 5 we show the electron momentum distribution at $t = 240T_p$.

The momentum density distribution in Fig. 5 can be shown to be practically constant after $t \approx 200T_p$. It seems to be well approximated by local power laws. The shown intervals in p_x may however be too narrow for an unambiguous identification of such a distribution.

The distribution grows steadily up to $\gamma \approx 0.4\gamma(v_b)$ which is comparable to the maximum γ the trapped blast shell electrons have reached in Fig. 3(a). Above $\gamma \approx 0.5\gamma(v_b)$ and up to $\gamma \approx 4\gamma(v_b)$ the momentum distribution goes over into a power law $N(\gamma) \sim N_0^{-1.3\gamma}$. At $4\gamma(v_b)$ we find a spectral break above which the distribution drops as $N(\gamma) \sim N_0^{-4.2\gamma}$ up to $\gamma \approx 10\gamma(v_b)$ at which $N(\gamma)$ becomes equivalent to a single computational electron. The power law distribution in Fig. 5 persists up to this peak momentum suggesting that in a physical plasma with 10^{13} times more electrons per volume element, the power law may extend to higher γ provided that the electrons can interact sufficiently long with the broadband oscillations in Fig. 2.

Separating the momentum distributions of species 1 and 3 reveals that the electron momentum distribution above $\gamma \approx 0.5\gamma(v_b)$ is determined by the oscillating dense beam of ISM electrons in Fig. 4(b). Because of their low density the blast shell electrons do not modify the spectrum in this momentum range.

In summary we have examined the development and the saturation of a two-stream instability where two cold plasmas, each consisting of protons and electrons, interpenetrate at a relative speed v_b with $\gamma(v_b) = 100$. One plasma may represent a thin fragment of a GRB blast shell or of an AGN jet and the second may be comparable to the ISM plasma into which this fragment expands. By assuming that the instability develops well behind the front of this fragment we could initialize all species in form of a spatially homogeneous distribution and we could use periodic boundary conditions for the simulation. The assumption of an unmagnetized plasma may be valid if the plasma expands along the magnetic field and if no electromagnetic instabilities develop.

The most unstable electrostatic wave grows in a narrow k interval and it saturates by forming initially a BGK mode with the blast shell electrons. The strong field of this BGK mode forces the ISM electrons onto a complicated phase space path. We have found that this BGK mode eventually collapses after which only broadband electrostatic fields are present. The interaction of the ISM electrons with these broadband waves leads to a momentum distribution that seems to follow a power law with a spectral break at which the exponent of the power law drops from -1.3 to -4.2. The peak momentum the ISM electrons reach does substantially exceed $\gamma(v_b)$ and could be substantially higher in a physical plasma due to the much larger particle numbers, provided the electrons can interact sufficiently long with the broadband waves to extend the power law to higher energies.

Future work has to assess the impact of a magnetic field and of a change of the density ratio between the blast shell plasma and the ISM plasma on the obtained results. The simulations also have to be extended to at least two spatial dimensions to examine how the growth of waves moving obliquely to the beam direction influences the simulation results.

We thank the Swedish National Supercomputer Centre (NSC) and the European Commission (Contract No. HPRN-CT-2001-00314) for their support.

*Electronic address: mardi@itn.liu.se
On leave from the Department of Science and Technology, Linköping University, 60174 Norrköping, Sweden.

[1] F. A. Aharonian *et al.*, Phys. Rev. D **66**, 023005 (2002).
[2] M. Pohl and R. Schlickeiser, Astron. Astrophys. **354**, 395 (2000).
[3] M. Pohl, I. Lerche, and R. Schlickeiser, Astron. Astrophys. **383**, 309 (2002).
[4] A. Panaitescu and P. Mészáros, Astrophys. J. **492**, 683 (1998).
[5] L. E. Thode and R. N. Sudan, Phys. Rev. Lett. **30**, 732 (1973).
[6] J. W. Eastwood, Comput. Phys. Commun. **64**, 252 (1991).
[7] O. Buneman, Phys. Rev. Lett. **1**, 8 (1958).
[8] J. B. Rosenzweig, Phys. Rev. A **38**, 3634 (1988).
[9] I. B. Bernstein, J. M. Greene, and M. D. Kruskal, Phys. Rev. **108**, 546 (1957).
[10] W. L. Kruer, J. M. Dawson, and R. N. Sudan, Phys. Rev. Lett. **23**, 838 (1969).